Scalable Processing of Moving Flock Patterns

Andres Oswaldo Calderon Romero
Pontificia Universidad Javeriana
Bogotá, Colombia
andrescalderonr@javeriana.edu.co

Vassilis Tsotras
University of California, Riverside
Riverside, USA
vtsotras@ucr.edu

Petko Bakalov
ESRI
Redlands, USA
pbakalov@esri.com

Marcos Vieira
Google
San Francisco, USA
mrvieira@gmail.com

Abstract

We present a scalable approach for identifying moving flock patterns in large trajectory databases. A moving flock pattern refers to a group of entities that move closely together within a defined spatial radius for a minimum time interval. We focus on improving the state-of-the-art sequential algorithms, which suffer from high computational costs when dealing with large datasets. By leveraging distributed frameworks and utilizing spatial partitioning, the proposed solution aims to significantly reduce the time required to detect moving flock patterns. We highlight the bottlenecks of the sequential approaches and offer optimizations like partition-based parallelism and strategies for managing flock patterns that span multiple partitions. An experimental evaluation using synthetic trajectory datasets, demonstrates that the proposed methods substantially improve scalability and performance compared to existing sequential algorithms.

CCS Concepts

• **Computing methodologies** → **Parallel algorithms**; **MapReduce algorithms**; • **Information systems** → **Data structures**.

Keywords

Mobile patterns

ACM Reference Format:
Andres Oswaldo Calderon Romero, Vassilis Tsotras, Petko Bakalov, and Marcos Vieira. 2025. Scalable Processing of Moving Flock Patterns. In *19th International Symposium on Spatial and Temporal Data (SSTD '25), August 25–27, 2025, Osaka, Japan.* ACM, New York, NY, USA, 11 pages. https://doi.org/10.1145/3748777.3748794

1 Introduction

Recent technological advances have dramatically increased the volume of spatio-temporal data collected from GPS devices, smartphones, and IoT systems. These datasets capture the movement of objects over time, providing valuable insights for various applications, including transportation management, urban planning, and ecological studies. However, detecting complex mobility patterns in such data remains a significant computational challenge.

Among those complex patterns, moving flock patterns refer to groups of objects that move together within a specific spatial radius for a minimum time interval. Detecting these patterns is computationally demanding because it involves tracking groups over multiple time instants, where the same entities remain within a defined proximity. A flock pattern is a set of at least μ entities that move together inside a fixed radius of diameter ε during minimal δ consecutive time intervals. This problem is known to be NP-hard [11], making it challenging for traditional algorithms to scale effectively with large datasets.

Early approaches, such as the Basic Flock Evaluation (BFE) algorithm [21], provided the first polynomial-time method for flock detection, but faced high computational costs due to frequent disk overlap checks and candidate evaluation. Despite improvements through frequent pattern mining [6] and plane sweeping techniques [18], these methods still struggle with scalability in dense datasets.

This work introduces a scalable approach for detecting moving flock patterns in very large and dense trajectory databases. Using distributed frameworks and spatial partitioning, the proposed method significantly reduces computation times and addresses critical limitations, including efficient handling of dense data regions, reduced disk replication overhead, and parallelized spatial-temporal joins. Experimental evaluations demonstrate substantial performance gains over state-of-the-art methods, validating the approach for large-scale trajectory data analysis.

2 Related Work

The rapid growth of location-based devices, such as GPS, smartphones, and RFID tags, has allowed the collection of vast spatiotemporal datasets. These datasets have become a critical resource for identifying interesting spatiotemporal aggregate/density based queries [1, 2, 12, 20, 24], including moving clusters [16], convoys [15], and flocks [4, 11]. Specifically, the BFE (Basic Flock Evaluation) algorithm [21] introduced a polynomial-time method to identify flock patterns by detecting disks with a predefined diameter (ε) at specific time instants. However, this approach is computationally expensive, with a complexity of $O(2n^2)$ per time step, due to the need to repeatedly identify and combine disk-based proximity relationships.

Efforts to improve this performance include frequent pattern mining [6] and plane sweeping [18] techniques, which reduce the overhead of disk combination but still rely on the core BFE strategy. Depth-first algorithms [3, 10] have also been proposed to identify maximal duration flocks, but these methods face scalability challenges in dense datasets.

Parallelism has emerged as a promising approach to improve performance, taking advantage of GPU-based methods [9] and cluster computing frameworks with spatial capabilities [7, 14, 23]. However,

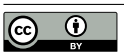

SSTD '25, Osaka, Japan

ACM ISBN /25/08
https://doi.org/10.1145/3748777.3748794

these techniques often suffer from memory and communication overheads, limiting their scalability for large datasets.

Despite these advancements, significant challenges remain in efficiently detecting moving flock patterns at scale, particularly in regions with high density and a large number of entities moving simultaneously. This work addresses these gaps by introducing a scalable partitioning and replication approach that significantly improves performance for large-scale, dense spatio-temporal datasets.

3 Background

We first provide an overview of the current state-of-the-art sequential approaches. This will enable highlighting their challenges and limitations in handling large spatio-temporal datasets, as described in the next Section.

3.1 The BFE sequential algorithm

The Basic Flock Evaluation (BFE) algorithm [21] was the first sequential approach designed to identify flock patterns in trajectory databases. Below, we provide a general overview of its key aspects.

It is important to note that the BFE algorithm operates in two phases. In the first phase, it identifies *maximal disks* at the current time step. A maximal disk is defined as a set of entities such that no proper subset of this set forms another disk, and no other disk can include this set without duplication. In the second phase, the algorithm extends and reports previous flocks by combining them with newly discovered disks.

The input for the first phase consists of a set of points, the query minimum distance ε (which defines the maximum diameter of the disks within which the moving entities must lie), and the minimum number of entities μ per disk. The primary objective of this phase is to identify a set of disks at each time step, facilitating their combination with future disks to form flocks, as flocks are defined by their persistence over a period of time.

The main steps within phase 1 follow:

(1) Pair finding: The algorithm uses the parameter ε to identify pairs of points that are within a maximum distance of ε units from each other. This is achieved through a distance self-join operation on the set of points, using ε as the distance threshold. To avoid redundancy, duplicate pairs are eliminated; for example, the pair (p_1, p_2) is considered identical to the pair (p_2, p_1), so only one instance is retained. Point IDs are used to filter out these duplicates efficiently.
(2) Center computation: From the set of pairs obtained, each pair is used to compute the centers of two circles, each with a radius of $\frac{\varepsilon}{2}$, whose circumferences pass through the two points in the pair.
(3) Disk finding: Once the centers have been identified, a query is executed to gather the points within a distance of ε units from each center. This is accomplished by performing a distance join between the set of points and the set of centers, using $\frac{\varepsilon}{2}$ as the distance parameter. As a result, each disk is defined by its center and the IDs of the surrounding points. At this stage, a filter is applied to discard any disks that contain fewer than μ entities.
(4) Disk pruning: It is possible for a disk to contain the same set, or a subset, of points as another disk. In such cases, the algorithm reports only that one disk which contains the other(s), referred to as the *maximal* disk.

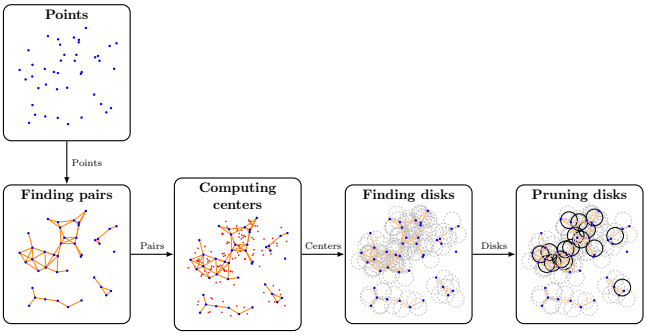

Figure 1: BFE Phase 1 steps on a sample dataset.

It is important to note that BFE also employs a grid structure in this phase to optimize spatial operations. The algorithm divides the space into a grid, where each cell has a side length of ε [21]. This structure allows BFE to limit its processing to each grid cell and its eight neighboring cells. There is no need to query cells beyond this neighborhood, as points in more distant cells are too far away to influence the results. Figure 1 shows an example of the Phase 1 steps using a sample dataset.

Phase 2 (the combination, extension and reporting of flocks) performs a recursion using the set of disks found at time i and the set of partial flocks computed at the previous time instant $i-1$. As we do not know where and how far a group of points can move in the next time instant, this step performs a (temporal) join between both sets (partial flocks computed at time $i-1$ and maximal disks found in time i). When a join is performed, we check that the number of common points remains greater than μ, in which case the partial flock extends in time. A flock is reported in the answer if its duration has reached the minimum duration δ; otherwise, it remains as partial flock and it will be further evaluated during the next iteration at the next time instant.

Similarly, Figure 2 illustrates the recursive process and how the set of partial flocks from previous time instants feeds into the next iteration. The example assumes a δ value of 3, meaning flocks start being reported from time instant t_2. Note that time instants t_0 and t_1 are considered the initial conditions. At the start of the algorithm, maximal disks are identified at t_0, which are immediately transformed into partial flocks with a duration of 1 and then passed on to the next time instant. At t_1, a new set of maximal disks $\mathcal{D}_1$ is found and joined with the partial flocks from t_0, denoted as $\mathcal{F}_0$. The information for each partial flock is updated accordingly, including its duration and the points it contains. From this point onward, subsequent time instants follow the exact steps outlined before.

3.2 The PSI sequential algorithm

The PSI algorithm, proposed by [18], follows a similar process to the BFE algorithm. However, instead of using a grid structure to index points within the area, PSI employs a sweep-line approach that processes points in order of their x-coordinates. For each visited point p, the algorithm considers a square of side length 2ε centered at p. It only examines the points to the right of p that lie within two half-squares of side length ε.

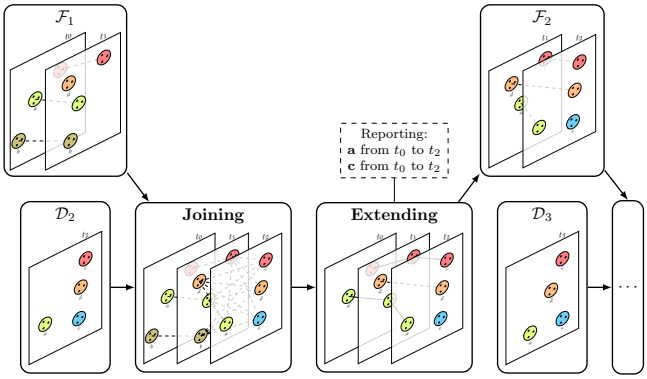

Figure 2: BFE Phase 2 example explaining the stages along time instants and the initial conditions.

While BFE processes points inside a grid cell of side length ε along with its eight neighboring cells, PSI focuses on the points in these two half-squares. As a result, PSI more efficiently identifies the points relevant for detecting candidate pairs, centers, and disks. This indexing method has been shown to outperform BFE in most cases, with BFE offering similar or better performance only when ε values are relatively small. In such cases, the number of points to consider is smaller, and PSI still requires sorting the points for the sweep-line approach. Therefore, both approaches are considered in the following sections.

4 Bottlenecks in the sequential approaches.

Since both sequential approaches follow the same steps , we will focus on discussing bottlenecks from both approaches using the BFE as an example. Certain stages in the BFE process are notably impacted when handling very large datasets, especially when large amount of trajectories happening at the same time are analyzed.

Phase 1: Spatial finding of maximal disks. Consider first Phase 1. As illustrated in Figure 1, this phase's steps are demonstrated using a sample dataset. It is important to note that the final set of maximal disks is significantly smaller than the initial number of candidate disks found. Specifically, the number of candidate centers to evaluate is $2|\tau|^2$, where τ represents the number of trajectories [21]. Our experiments reveal that this issue becomes more pronounced not only in very large datasets but also in those containing areas with a high density of moving entities.

Phase 1: Handling high-density areas. Even though partitioning the problem into smaller subareas can improve performance by exploiting parallelism and reducing the number of trajectories that need to be analyzed, a few subareas (i.e., partitions) may still exhibit low performance. This issue arises due to how the trajectories are distributed within the subarea. We could have small areas with a relatively low number of trajectories, but if these trajectories are densely concentrated in a specific region, we still face an explosion in the number of candidates. This, in turn, increases the response time required to evaluate, filter, and find the maximal disks. This phenomenon directly impacts parallelism because these few high-density subareas will dominate the overall execution time.

Phase 2: Dealing with partial flocks during the temporal join. At the end of Phase 1, we have computed a set of maximal disks for a given time instant. In Phase 2, we proceed by combining these disks over time instants to form flocks. However, since Phase 1 involved partitioning the spatial domain for parallelism, Phase 2 becomes more complex as flocks can move across spatial partitions over time. Once the maximal disks are identified for a time instant i, a temporal join occurs within each partition to link these disks with partial flocks from the previous time instant $(i-1)$. However, we must account for partial flocks that may appear near the partition borders and potentially move into adjacent partitions.

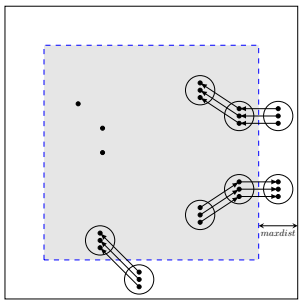

Figure 3: Examples of partial flocks that that start or end in the border area of a partition.

5 Scalable Solutions

5.1 Finding maximal disks using a *divide & conquer* approach

To address the first issue stated at section 4, we propose a *divide & conquer* strategy that partition the study area into smaller subareas, allowing for independent and parallel evaluation. The strategy consists of three key steps: first, the *partition and replication* stage, followed by the *local flock discovery* within each partition, and finally, the *filtering stage*, where we consolidate and unify the results. Each of these steps is detailed below.

- Partition and Replication: Figure 4 provides a brief example of the partition and replication stage. Different types of spatial indexes, such as grids, R-trees, or quadtrees, can be used to create spatial partitions of the input dataset. In the example shown in Figure 4.b, we use a quadtree, which generates seven partitions. To ensure each partition can locally identify flocks, it must have access to all relevant data. This is achieved by replicating points that are within a distance of ε from the border of each partition, an area referred to as the *expansion zone*, into adjacent partitions. Figure 4.c illustrates each partition, surrounded by a dotted line representing the expansion zone, which includes the points that need to be replicated from neighboring partitions.
- Local flock discovery: At this stage, each partition can be processed independently and in parallel, with partitions assigned to different processing nodes. Within each partition, we can execute the steps of Phase 1 of the BFE algorithm locally.
- Filtering: While partitioning and replication facilitate parallelism, they can also lead to result duplication, as different nodes may report the same maximal disk. Specifically, if a disk's center lies within a partition, it will be reported only

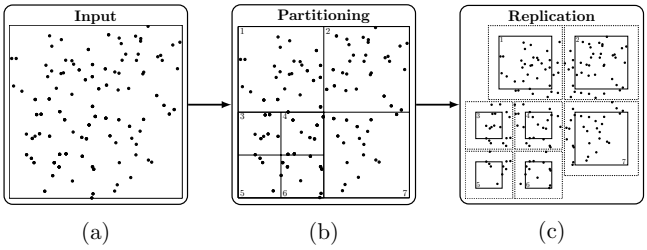

Figure 4: An example of partitioning and replication on a sample dataset.

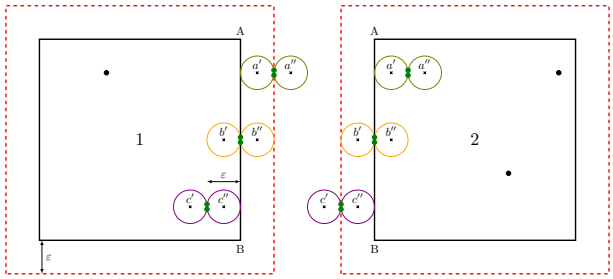

Figure 5: Ensuring no loss of data in safe zone and expansion area.

once by the node processing that partition. However, disks with centers located in an expansion zone will be reported by all partitions that share that zone. To address this, we propose a reporting approach that effectively prevents such duplication, which we detail below.

Disks with centers in an expansion zone are created by points that exist in both partitions due to replication. We assert that each partition should only report disks generated within its own area and not those originating in its expansion zone. Figure 5 illustrates the possible scenarios. Assume partitions 1 and 2 in the figure are contiguous, sharing edge AB. Consider the disks a' and a'' (each with a diameter of ε), which are generated by two points (shown in green) located in the expansion zone of partition 1 but inside partition 2. In this case, both a' and a'' will be reported by partition 2. Similarly, both c' and c'' will be reported by partition 1. However, b' will be reported by partition 1, while b'' will be reported by partition 2.

5.2 Addressing density challenges using maximal cliques.

As we discussed in section 4, dense areas pose challenges for pruning, as they are highly sensitive to increases in the value of ε, leading to an exponential growth in the number of pairs. To address this, we explored alternative strategies that could enable more effective grouping of points. It is important to note that density-based spatial clustering methods, such as DBSCAN [8], are not suitable for this problem. In very dense regions, these approaches often produce a single large cluster, which does not resolve the issue. Additionally, clustering algorithms do not enforce the strict relationships required for a flock, where all points must be within a distance of ε from each other.

Instead, we explored graph-oriented clustering, focusing on the concept of *maximal cliques*. In an undirected graph, a *maximal clique* is a subset of vertices where each vertex is directly connected to every other vertex in the subset. Additionally, the clique is maximal in the sense that it cannot be extended by adding more vertices [5, 19].

In this context, the points within a partition can be treated as the vertices of an undirected graph, where edges are created between pairs of points that are within a distance of ε. By finding the set of maximal cliques in this graph, we identify subsets of points where each point is connected to all others in the subset. This means that all points in the clique are at most ε apart, and no additional points can be added to the subset. However, not every maximal clique qualifies as a maximal disk. A maximal clique becomes a maximal disk only if it contains at least μ points and can be enclosed by a disk with a radius of $\frac{\varepsilon}{2}$.

To verify whether a maximal clique qualifies as a maximal disk, we use the concept of the *Minimum Bounding Circle* (MBC) [22]. Given a set of points in Euclidean space, the MBC is the smallest circle that can enclose all the points. For each maximal clique identified within a partition, we can quickly check if all points in the clique fit within an MBC with a diameter of ε. If they do, we can immediately report the set of points and their MBC as a maximal disk. However, cliques that do not satisfy this condition must be evaluated using the traditional method. This involves computing the potential disk centers, identifying candidate disks, and pruning them.We have termed this approach as CMBC. We evaluate the performance of the CMBC approach later in the experimental section.

5.3 Handling issues in the temporal domain

To address the last issue presented in section 4, we introduce an additional parameter, *maxdist*, which represents the maximum distance a moving object can travel between consecutive time instants (see Figure 3). We define the *safe area* of a partition as the internal region that is at least *maxdist* away from the partition's border (illustrated in grey in Figure 3). Any partial or full flocks discovered within a partition's safe area can be directly reported as results. However, flocks that start or end outside the safe area must be collected for post-processing to determine if they correspond with partial flocks from neighboring partitions. These cases, where flocks cross between partitions, are referred to as *crossing partial flocks* (CPFs).

In Figure 6, we observe an example that illustrates the possible cases. The figure shows flocks b and d, which start and end within the safe area of the orange partition; both flocks are ready to be reported.

On the other hand, flocks a and c move across different partitions. Flock a begins in the blue partition at t_0 and moves to the orange partition at t_2. This movement results in two CPFs: a', from t_0 to t_1, reported by the blue partition, and a'', from t_2 to t_4, reported by the orange partition.

Similarly, flock c starts in the blue partition at t_0, moves to the orange partition at t_2, and returns to the blue partition at t_3. This creates three CPFs: c', from t_0 to t_1, reported by the blue partition;

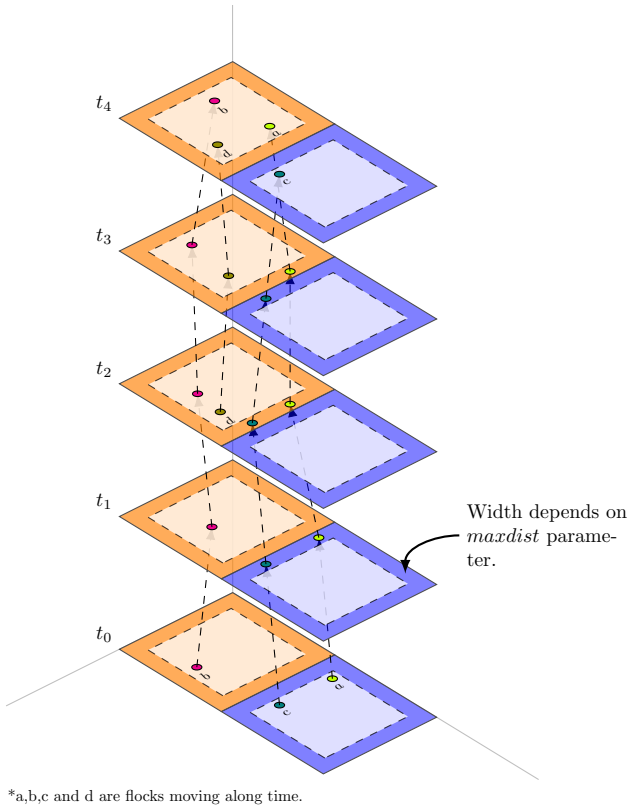

Figure 6: CPFs cases moving along different partitions over time.

c'', at t_2, reported by the orange partition; and c''', from t_3 to t_4, reported by the blue partition.

In the post-processing stage, we evaluate four alternatives for collecting and checking crossing partial flocks (CPFs). The simplest approach is to gather all CPFs and process them sequentially on a single node (the master node). However, due to the large number of partitions and the *maxdist* parameter, the volume of CPFs requiring post-processing can become substantial, leading to a bottleneck that negatively impacts overall performance.

We also evaluate an intermediate approach where the CPFs from a given partition are sent to a middle-level node for processing, based on the quadtree structure used to create the partitions. The choice of which middle-level node to send the CPFs to is determined by a user-defined parameter called *step*. A value of $step = 1$ corresponds to sending CPFs to the immediate parent, $step = 2$ to the grandparent, and so on, until the root is reached. For example, with *step=1*, all CPFs from a partition are first sent to its parent node in the quadtree. The parent node processes its CPFs, but some flocks may still cross outside the parent's safe area. These leftover CPFs are then passed to the next parent (since $step = 1$), and this process continues until all CPFs are processed, potentially reaching the root node. This approach allows for parallelism in post-processing, as moving to a parent node increases the partition's area and improves the likelihood that CPFs can be resolved at that level. In the experimental section, we test different values of the *step* parameter,

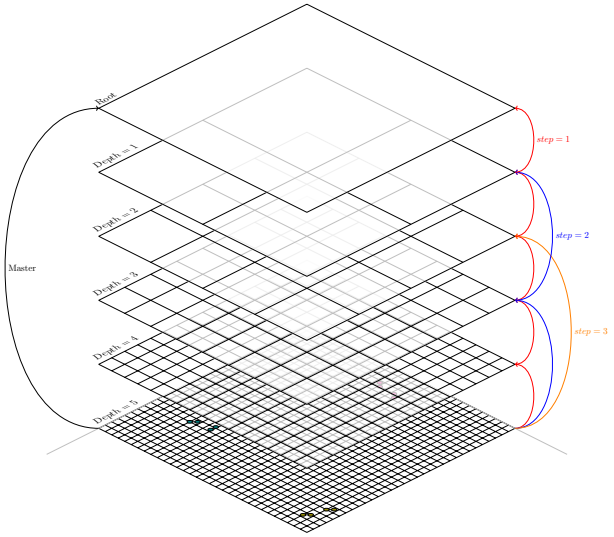

Figure 7: Master and By-Level alternatives. Different values of *steps* are illustrated for the By-Level apprach,

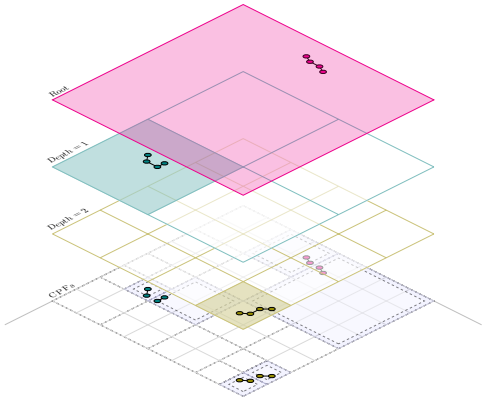

Figure 8: LCA alternative and how it resolves CPFs at the nearest shared ancestor of the involved partial flocks.

such as $step = 2$, where CPFs are sent to the grandparent at each stage. Figure 7 illustrates the Master and By-Level alternatives.

Unlike the previous two approaches, which assign all CPFs from a given partition in the same way (partition-based), the third alternative assigns each CPF individually (CPF-based). For a given CPF f, we extend its most recent disk by a ring with a size of *maxdist*, identifying all overlapping partitions for this extended disk —essentially determining which neighboring partitions the objects in f could move to in the next time instant. For each overlapping partition, we retrieve the Least Common Ancestor (LCA) between that partition and f's original partition. CPF f is then sent to the node(s) corresponding to these LCAs. The benefit of this approach is that the LCA can efficiently complete the processing for f, as it exploits proximity using *mindist* (see Figure 8). However, the downside is the increased copying overhead, as f may need to be sent to multiple nodes.

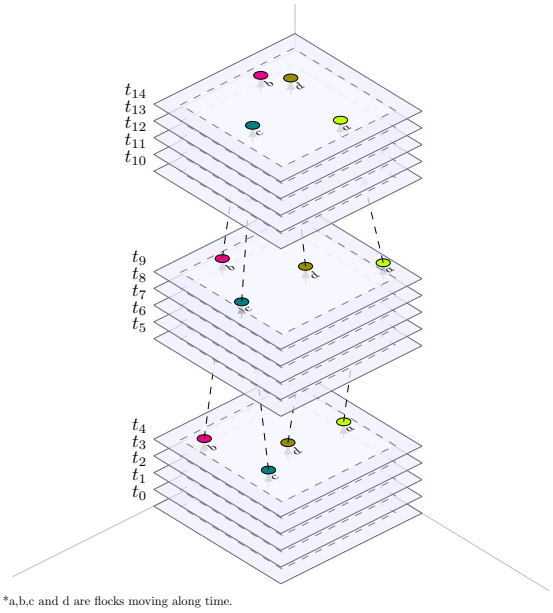

Figure 9: An alternative division on the time dimension to partition the data into cubes.

A limitation of the previous alternatives is that each spatial partition is processed by a single node, which incrementally evaluates all time instances for that partition. The fourth alternative introduces fixed divisions in the temporal domain, based on a user-defined parameter (number of divisions), as illustrated in Figure 9. In this approach, the spatio-temporal space is divided into temporal 'cubes,' each of which can be processed by different nodes. For simplicity, we assume that each division spans the same length of time. However, an additional validation step is required to ensure continuity of flocks across temporal divisions.

6 Experimental Evaluation

6.1 Experimental Setup

For our experiments, we utilized a 12-node cluster, each running Linux (kernel version 3.10) and Apache Spark 2.4. Each node was equipped with 8 cores, providing a total of 96 cores across the cluster. Each core operated with an Intel Xeon CPU at 1.70 GHz, and each node had 4 GB of main memory.

To evaluate the different approaches, we generated three synthetic datasets with varying characteristics, as detailed in Table 1. These datasets were created using the SUMO simulator [17], by importing traffic networks of Berlin and Los Angeles from OpenStreetMap [13]. We configured SUMO for pedestrian traffic and generated datasets of 10K, 25K, and 50K pedestrian trajectories. The total duration of the trajectories was set to 10, 30, and 60 minutes, respectively, with positions of pedestrians recorded at one-minute intervals.

For the partitioning phase, we employed a quadtree structure, though other indexing methods could also be used. The advantage of using a quadtree is its ability to create nodes that tend to have a similar number of objects. The input to this phase is a set of points

Table 1: Description of datasets.

Dataset	Number of Trajectories	Total number of points	Maximum Duration (min)
Berlin10K	10000	97526	10
LA25K	25000	1495637	30
LA50K	50000	2993517	60

in the format *(traj-id, x, y, t)*. To construct the quadtree, we begin by sampling 1% of the input data and inserting this subset into an initially empty quadtree.

A key parameter for the quadtree is the node capacity, denoted as c. When the number of points in a node exceeds this capacity, the node splits. After all the sampled points are inserted, we use the Minimum Bounding Rectangles (MBRs) of the leaf nodes as the partitions for our approach. The remaining points are then inserted into these fixed partitions, with no further splits occurring. Each partition is assigned to a different cluster node, where a sequential version of either BFE or PSI is executed locally on the points within that partition.

6.2 Optimizing the number of partitions for Phase 1.

The capacity parameter c directly influences the number of partitions in the quadtree. A smaller value of c results in a higher number of partitions, which leads to many smaller tasks that can be distributed across the cluster. However, this can increase the overhead associated with data transmission and, potentially, replication, which may become a bottleneck. Conversely, a larger value of c reduces the number of partitions, resulting in fewer but larger tasks. This increases the workload of the sequential algorithm within each partition, potentially extending the response time for individual jobs.

Figure 10 presents the execution time (in seconds) for computing maximal disks (Phase 1) at a specific time instant, using different values of c and ε. The experiments were conducted using the LA25K dataset. For the case where $\varepsilon = 20m$, we observe that there is an optimal value of c that minimizes the execution time for finding maximal disks, which occurs at $c = 100$ (corresponding to approximately 1300 partitions). Additionally, the optimal value of c varies based on the value of ε. For instance, with a smaller $\varepsilon = 2m$, the execution time is minimized at a larger capacity $c = 500$ (around 250 partitions). When ε is large, more pairs of points need to be processed, resulting in a higher number of maximal disks to compute. In such cases, using a smaller value of c creates more partitions within the same spatial area, thereby distributing the workload more evenly across partitions and reducing the amount of work per partition.

After determining the optimal value of c for a given ε, we further analyzed the behavior of BFE and PSI on the most 'demanding' partitions, those that required the longest time to complete Phase 1. Since the partitions are processed in parallel across different cores, these demanding partitions have the greatest impact on the overall performance. By focusing on these partitions, we can better understand potential bottlenecks and further optimize the system's efficiency.

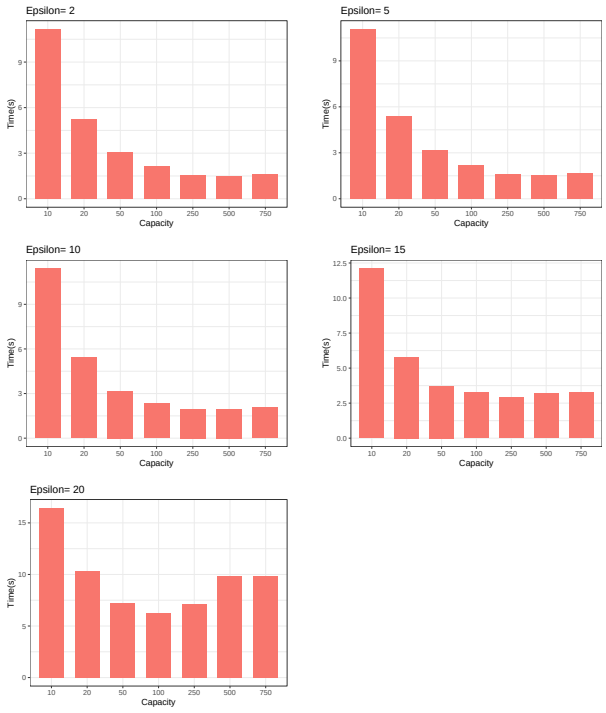

Figure 10: Execution time testing different values for Capacity (c) and Epsilon (ε).

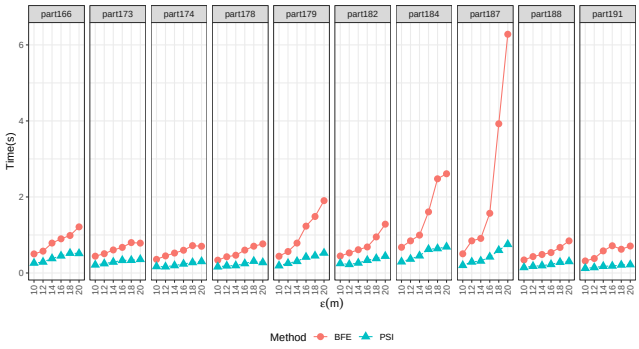

Figure 11: Comparison of PSI and BFE algorithms for the most time-consuming partitions when ε varies from 10 to 20 meters. The results demonstrate that PSI consistently outperforms BFE due to its more flexible bounding box approach, which reduces candidate pair evaluations in dense partitions.

6.3 Analyzing most costly partitions.

We began by identifying the top 10 partitions that required the most time to execute the BFE algorithm with $\varepsilon = 20$ meters. For these specific partitions, we ran both BFE and PSI while varying ε from 10 to 20 meters. The Phase 1 execution times are shown in Figure 11, where it is evident that PSI consistently outperformed BFE across all values of ε.

We further investigated the reasons behind some partitions taking longer to compute. Figure 12 shows the Phase 1 execution times

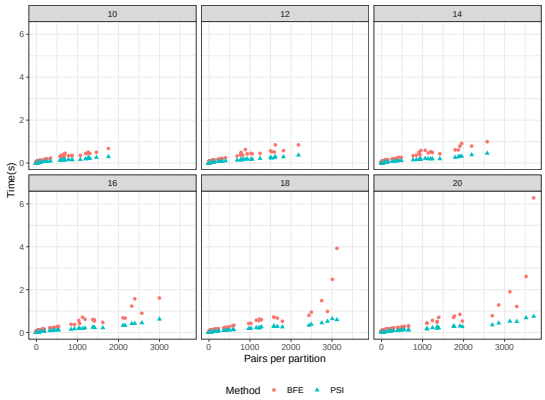

Figure 12: Execution time for pairs/disks finding in the dense partition.

per partition while varying ε from 10m to 20m, with partitions ordered by the number of pairs they contain. One key observation is that as ε increases, the number of pairs also increases, since a larger ε allows for more maximal disks. For instance, with $\varepsilon = 10m$, the maximum number of pairs in a partition is around 1800, whereas for $\varepsilon = 20m$, some partitions contain nearly 4000 pairs.

Another notable observation is that BFE is more sensitive to the density of pairs within a partition than PSI, a difference that becomes more pronounced at higher values of ε (e.g., 18m or 20m). As mentioned earlier, the flexible bounding boxes used by PSI more effectively isolate the relevant points for computing pairs, whereas BFE relies on a fixed grid cell, which makes it less efficient in denser partitions.

A final observation is that a few partitions take significantly more time than others, particularly those with a higher density of pairs. This is directly related to the number of maximal disks that need to be computed and subsequently pruned. For example, the partition that takes the longest time when $\varepsilon = 20m$ is the one with the highest number of pairs, which corresponds to partition 187 in Figure 11.

We further analyzed how Phase 1 processing is distributed within the most demanding partition. Figure 13.a (for BFE) and Figure 13.b (for PSI) display the time taken by each Phase 1 stage (refer to Figure 1) for partition 187. The most resource-intensive stage in both cases is the final step of filtering the disks, where disks whose points are contained within others are removed—this stage identifies the *maximal* disks (labeled as 'Maximals' in the figure).

This stage is particularly costly because both BFE and PSI must scan a large set of candidate disks, identifying and removing those that are redundant. As ε increases, this processing becomes even more time-consuming, as the number of pairs and candidate disks grows along with ε.

6.4 Can we reduce pruning time?

In this section we evaluate the CMBC approach introduced in section 5.2. In this approach, we use maximal cliques algorithms to group points in dense areas and we check if those maximal cliques are enclosed by MBC with radius lower than $\frac{\varepsilon}{2}$ to quickly report them as maximal disks. In order to evaluate the group of cliques

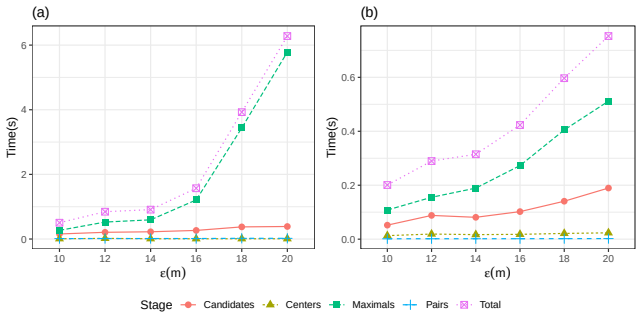

Figure 13: Processing time for the stages of Phase 1, in (a) standard BFE and (b) standard PSI.

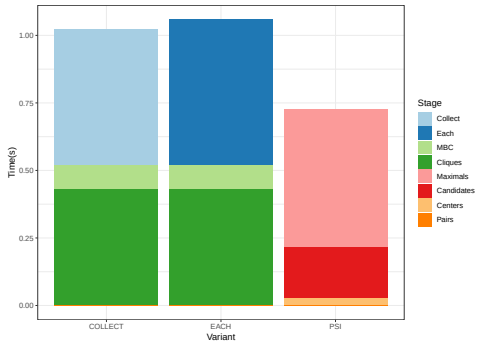

Figure 14: Execution time of CMBC variants compared to standard PSI in the partition 187 ($\varepsilon = 20m$).

that do not meet the above condition, we implemented two variants. The first variant, termed *COLLECT*, gathers the points from all cliques that are not reported as maximal disks, removes duplicates (since points may appear in multiple cliques), and then applies the traditional pruning method to the entire set. In the second variant, *EACH*, we apply the pruning procedure independently for each clique that does not qualify as a maximal disk.

Figure 14 compares the performance of the two CMBC variants with the time taken by PSI for the same stage. Interestingly, neither variant achieves a reduction in execution time. Upon closer examination, it becomes evident that while identifying the cliques and their MBCs is relatively fast, only a small fraction of the cliques qualify as maximal disks. Consequently, the overhead associated with processing the remaining cliques outweighs the benefits, making the original PSI approach more efficient.

We next increased the density of points within the same partition to determine whether a higher number of cliques would qualify as maximal disks and thus affect the performance. The number of points in the partition was incrementally increased from 500 (the initial number) to 1K, 2K, 4K, and 6K so as to test varying densities. For each simulation, we recorded the execution time required to identify maximal disks, increasing the value of ε from 10 to 20 meters. Additionally, we tracked the number of pairs generated for each value of ε as a measure of candidate disk density. Figure 15 presents the performance of CMBC (using the COLLECT variant) compared to PSI as the number of points and pair density increased.

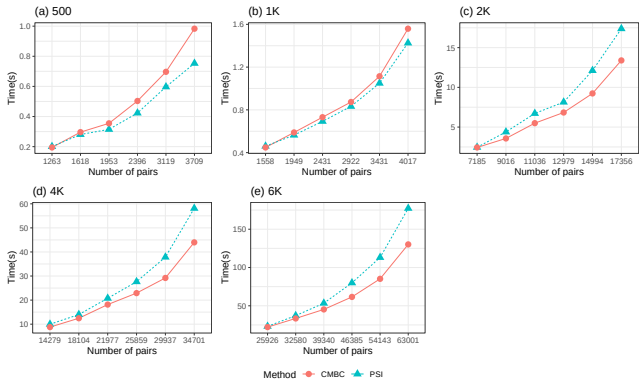

Figure 15: Execution time comparison of the CMBC approach (COLLECT variant) and the standard PSI algorithm as the number of points and pair density increase within a partition.

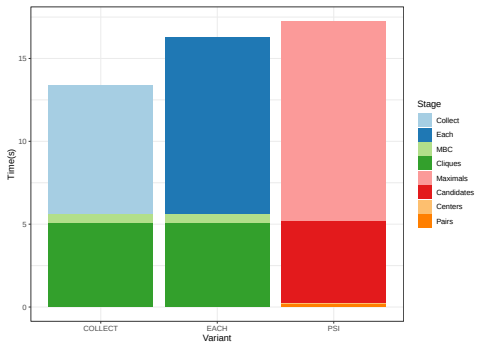

Figure 16: Execution time of the CMBC variants compared to standard PSI in the partition 187 with ≈2K points present ($\varepsilon = 20m$).

We observed that the performance of the CMBC approach surpasses that of PSI when the partition contains more than 2K points and the pair density increases. To further investigate, we evaluated the behavior of both CMBC variants for a partition with 2K points, as shown in Figure 16. The results demonstrate that the COLLECT variant outperforms PSI in this scenario. The higher density led to a greater number of cliques being identified early as maximal disks. This early identification significantly reduced the number of pairs and candidates that needed evaluation through the traditional pruning approach, thereby improving overall efficiency.

6.5 Relative performance of BFE and PSI Phase 1 using synthetic datasets.

To further examine the relative performance of the scalable BFE and PSI approaches for Phase 1, we also conducted experiments using a synthetic dataset where we could control the values of c, ε, and point density. We used a fixed square area of 1000m x 1000m, within which we uniformly distributed 25K, 50K, 75K, and 100K points.

We experimented with different quadtree capacities (c values of 100, 200, and 300), which resulted in varying numbers of partitions

Table 2: Number of partitions by capacity and number of points in synthetic uniform datasets.

	25K	50K	75K	100K
c=100	544	1024	1024	2185
c=200	256	514	1024	1024
c=300	256	514	481	1024

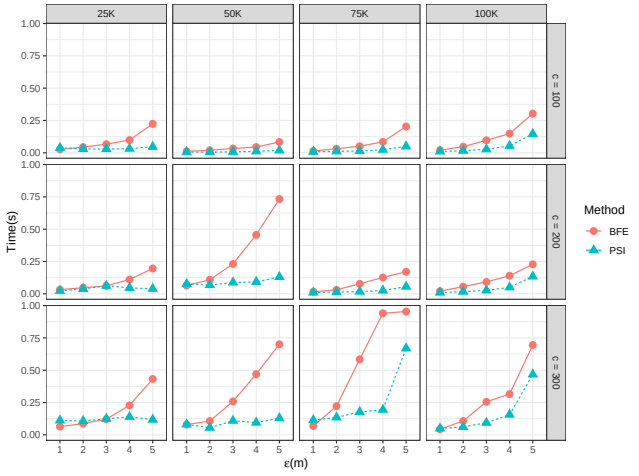

Figure 17: Performance in an uniform dataset analysing density and capacity with diverse values for epsilon.

(as shown in Table 2). Both BFE and PSI were tested for phase 1, where maximal disks are identified, using ε values ranging from 1m to 5m. The results are presented in Figure 17.

Overall, PSI demonstrated better performance than BFE, though there were cases (particularly with smaller ε values) where BFE outperformed PSI. In these cases, the smaller ε generates fewer pairs, and the additional ordering step required by PSI becomes an overhead. However, in the subsequent experiments focusing on temporal joins (phase 2, flock creation), we concentrate on the scalable performance of PSI.

6.6 Evaluation of Phase 2: Temporal join.

Phase 2 focuses on joining maximal disks across time instants to form flocks. In Section 4, we discussed four alternatives: Master, By-Level, LCA, and Cube-based. For these experiments, we used the scalable PSI approach due to its robust performance. First, we compared the Master and By-Level alternatives while varying ε from 20m to 40m using the Berlin10K dataset (see Figure 18). For the By-Level approach, we tested different step values ranging from 1 to 6. The Master approach proved to be the slowest, due to the overhead of sending all CPFs to the root node. The performance of the By-Level approach depends on the step size. A smaller step value (e.g., step 1) introduces overhead because CPFs may need to be evaluated at more intermediate nodes before completion. On the other hand, a larger step value reduces parallelism by sending more CPFs to intermediate nodes. Based on these experiments, we determined that Step=3 offers the best balance.

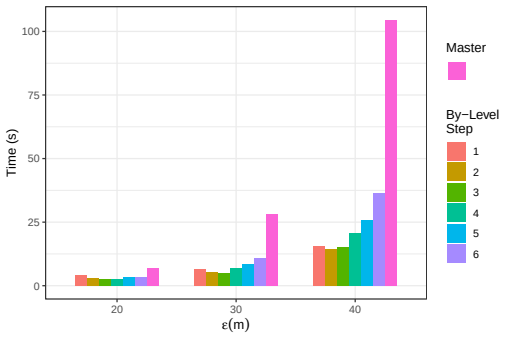

Figure 18: Root and step alternative for temporal join using the Berlin dataset.

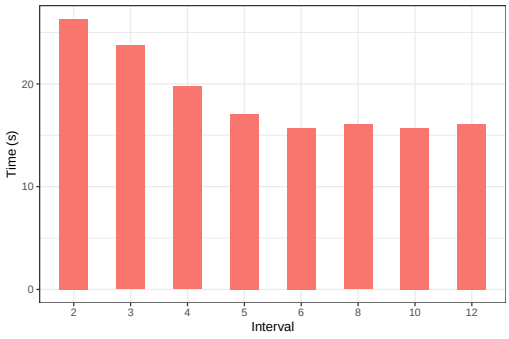

Figure 19: Interval optimization for the Cube-based alternative for temporal join using the LA25K dataset.

We also evaluated the optimal value for the *interval* parameter in the Cube-based approach. Using the LA25K dataset with $\varepsilon = 30m$, we tested various interval values, ranging from 2 to 12 time instants. This dataset contains 30 time instants in total. The results, shown in Figure 19, illustrate the trade-offs involved. Lower interval values result in higher parallelism, as more cubes can be processed independently. However, this also increases the number of cube crossings for CPFs that need to be checked, which adds to the execution time. Conversely, larger interval values reduce parallelism but also decrease the number of CPF crossings. Based on these findings, we selected $interval = 6$ as the optimal value for the Cube-based approach.

Finally, we compared the optimized versions of the By-Level and Cube-based approaches with the Master and LCA methods. Figure 20 shows the results, including the sequential PSI algorithm as a reference. This experiment was conducted using the LA25K dataset with ε values ranging from 5m to 30m. Clearly, all parallel approaches offer significant improvements over the sequential PSI.

To further analyze the relative performance of the scalable approaches, Figure 21 focuses on the parallel algorithms for the same experiment. Interestingly, for very small ε values, the Master approach performs best —primarily because the limited number of flocks makes sending the CPFs to a single node fast and efficient. However, as ε increases, the Cube-based approach becomes the most effective, leveraging greater parallelism. By-Level also improves over the Master approach as ε grows, as explained in Figure

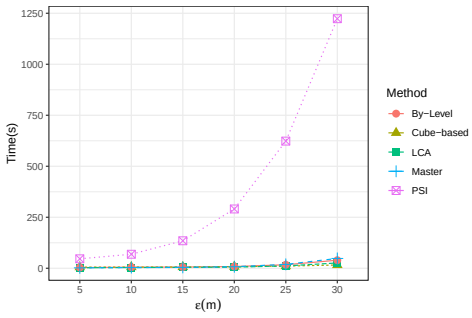

Figure 20: Performance comparing parallel and sequential alternatives in the LA25K dataset.

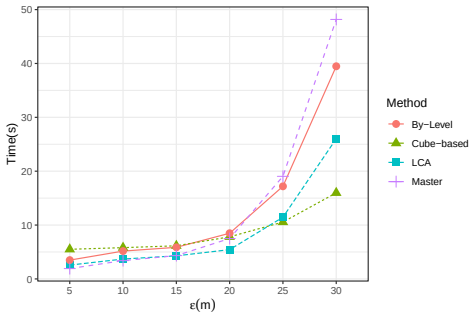

Figure 21: Performance of the 4 parallel alternatives in the LA25K dataset.

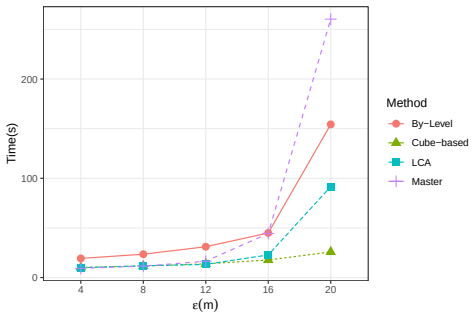

Figure 22: Performance of the 4 parallel alternatives in the LA50K dataset.

18. Similarly, for larger ε values, the LCA approach outperforms By-Level because it more quickly identifies the node that can complete the CPF operations.

We repeated the same experiment with the LA50K dataset, varying ε from 4m to 20m. The results, shown in Figure 22, once again demonstrate that the Cube-based approach offers the best performance as ε increases.

7 Conclusions

We presented a novel, scalable approach to discover moving flock patterns in large trajectory databases. By leveraging distributed frameworks, the proposed method overcomes the limitations of sequential algorithms that struggle with large-scale spatio-temporal datasets. Through partitioning and replication, as well as improvements in pruning and temporal joins, this approach efficiently handles dense data, offering significant performance improvements over traditional methods. The evaluation results demonstrate the scalability and effectiveness of the approach, making it a valuable contribution for analyzing complex movement patterns.

Acknowledgements: This research was partially supported by the US National Science Foundation grant IIS-1954644 and by NIFA award 2024-67022-43695.

References

[1] Laila Abdelhafeez, Andres Calderon, Amr Magdy, and Vassilis J. Tsotras. 2024. Pyneapple-G: Scalable Spatial Grouping Queries. *Proc. VLDB Endow.* 17, 12 (2024), 4469–4472. doi:10.14778/3685800.3685902

[2] Laila Abdelhafeez, Amr Magdy, and Vassilis J. Tsotras. 2023. SGPAC: generalized scalable spatial GroupBy aggregations over complex polygons. *GeoInformatica* 27, 4 (2023), 789–816. doi:10.1007/S10707-023-00491-8

[3] H. Arimura, T. Takagi, X. Geng, and T. Uno. 2014. Finding All Maximal Duration Flock Patterns in High-Dimensional Trajectories. (2014).

[4] M. Benkert, J. Gudmundsson, F. Hübner, and T. Wolle. 2008. Reporting Flock Patterns. *Computational Geometry* 41, 3 (2008), 111–125.

[5] C. Bron and J. Kerbosch. 1973. Algorithm 457: finding all cliques of an undirected graph. *Commun. ACM* 16, 9 (1973), 575–577.

[6] A. Calderon. 2011. *Mining Moving Flock Patterns in Large Spatio-Temporal Datasets Using a Frequent Pattern Mining Approach.* Master's thesis. University of Twente.

[7] A. Eldawy. 2014. SpatialHadoop: Towards Flexible and Scalable Spatial Processing Using Mapreduce. In *SIGMOD PhD Symposium*. 46–50.

[8] Martin Ester, Hans-Peter Kriegel, Jörg Sander, and Xiaowei Xu. 1996. A density-based algorithm for discovering clusters in large spatial databases with noise. In *Proceedings of the Second International Conference on Knowledge Discovery and Data Mining* (Portland, Oregon) *(KDD'96)*. AAAI Press, 226–231.

[9] M. Fort, J. Antoni, and N. Valladares. 2014. A Parallel GPU-Based Approach for Reporting Flock Patterns. *IJGIS* 28, 9 (2014), 1877–1903.

[10] X. Geng, T. Takagi, H. Arimura, and T. Uno. 2014. Enumeration of Complete Set of Flock Patterns in Trajectories. In *IWGS*. 53–61.

[11] J. Gudmundsson and M. van Kreveld. 2006. Computing Longest Duration Flocks in Trajectory Data. In *ACM SIGSPATIAL*. 35–42.

[12] M. Hadjieleftheriou, G. Kollios, and V.J. Tsotras. 2003. Performance Evaluation of Spatio-temporal Selectivity Estimation Techniques. In *Proceedings of the 15th International Conference on Scientific and Statistical Database Management (SSDBM 2003)*. 202–211. doi:10.1109/SSDM.2003.1214981

[13] Mordechai Haklay and Patrick Weber. 2008. Openstreetmap: User-generated street maps. *IEEE Pervasive computing* 7, 4 (2008), 12–18.

[14] J. Hughes, A. Annex, C. Eichelberger, A. Fox, A. Hulbert, and M. Ronquest. 2015. GeoMesa: a distributed architecture for spatio-temporal fusion. In *Defense + Security Symposium*.

[15] H. Jeung, M. Yiu, X. Zhou, C. Jensen, and H. Shen. 2008. Discovery of Convoys in Trajectory Databases. *VLDB* 1, 1 (2008), 1068–1080.

[16] P. Kalnis, N. Mamoulis, and S. Bakiras. 2005. On Discovering Moving Clusters in Spatio-Temporal Data. In *ASTD*. Springer, 364–381.

[17] Daniel Krajzewicz, Jakob Erdmann, Michael Behrisch, and Laura Bieker. 2012. Recent Development and Applications of SUMO - Simulation of Urban MObility. *International Journal On Advances in Systems and Measurements* 5, 3&4 (Dec. 2012), 128–138.

[18] P. Tanaka, M.. Vieira, and D. Kaster. 2016. An Improved Base Algorithm for Online Discovery of Flock Patterns in Trajectories. *JIDM* 7, 1 (2016).

[19] Etsuji Tomita, Yoichi Sutani, Takanori Higashi, Shinya Takahashi, and Mitsuo Wakatsuki. 2010. A Simple and Faster Branch-and-Bound Algorithm for Finding a Maximum Clique. In *WALCOM: Algorithms and Computation*, Md. Saidur Rahman and Satoshi Fujita (Eds.). Springer Berlin Heidelberg, Berlin, Heidelberg, 191–203.

[20] Reaz Uddin, Mehnaz Tabassum Mahin, Payas Rajan, Chinya V. Ravishankar, and Vassilis J. Tsotras. 2023. Dwell Regions: Generalized Stay Regions for Streaming and Archival Trajectory Data. *ACM Trans. Spatial Algorithms Syst.* 9, 2 (2023), 9:1–9:35. doi:10.1145/3543850

[21] M. Vieira, P. Bakalov, and V. Tsotras. 2009. On-Line Discovery of Flock Patterns in Spatio-Temporal Data. In *ACM SIGSPATIAL*. 286–295.

[22] E. Welzl. 1991. Smallest enclosing disks (balls and ellipsoids). In *New Results and New Trends in Computer Science*. Springer, 359–370.

[23] D. Xie, F. Li, B. Yao, G. Li, L. Zhou, and M. Guo. 2016. Simba: Efficient In-Memory Spatial Analytics. In *ICMD*. 1071–1085.

[24] D. Zhang and V.J. Tsotras. 2005. Optimizing spatial Min/Max aggregations. *VLDB J.* 14, 2 (2005), 170–181. doi:10.1007/S00778-004-0142-4